TIFONE: a design-oriented code for the inter-wrapper flow and heat transfer in liquid metal-cooled reactors

TIFONE: A DESIGN-ORIENTED CODE FOR THE INTER-WRAPPER FLOW AND HEAT TRANSFER IN LIQUID METAL-COOLED REACTORS

G.F. NALLO[1], G. GRASSO[2], F. LODI[2]

[1]NEMO Group, Dipartimento Energia, Politecnico di Torino, Torino, Italy
[2]ENEA (Italian National Agency for New Technologies, Energy and Sustainable Economic Development), Bologna, Italy

Email contact of corresponding author: giuseppefrancesco.nallo@polito.it

Abstract

The core of Lead-cooled Fast Reactors (LFRs) exploiting the closed sub-assembly (SA) option must be designed avoiding cold by-passes and preventing excessive thermal gradients among opposite faces of the assembly ducts. This requires a suitable coolant flow outside the assemblies themselves, in the so-called inter-wrapper (IW) region, for which the IW gap is determined by the core thermo-mechanical design. Moreover, for wrapped assemblies, the opportunity to introduce flow restrictions to tune the IW flow fraction at the SA level provides the designer with an extra degree of freedom, possibly allowing to reduce temperature differences at the outlet of the assemblies. Therefore, the designer needs to be aware of the axial and radial temperature profiles of the IW coolant throughout the whole core (i.e. including all core SAs), as well as of the axial and perimetrical temperature profiles of the wrapper of each SA. Notably, the possibly different temperature values of each side of the wrapper itself should be assessed, since they could induce SA bowing. To address these needs, a Design-Oriented Code (DOC), TIFONE, was developed and verified in compliance with ENEA software quality assurance requirements. TIFONE adopts the sub-channel method, leading to a sufficient level of spatial resolution while retaining the key features of a DOC, namely equilibrium, a low computational time and a clear application domain. The paper describes the code structure, governing equations and solution method. It also reports a preliminary validation against data from inter-wrapper flow and heat transfer experiments performed in the frame of the SESAME project at the THESYS loop within KALLA laboratory, confirming the code capability to reproduce the measured data in its anticipated validity domain.

1. INTRODUCTION

The development of Heavy Liquid Metal Cooled Reactors (HLMCRs) is currently being pursued within the framework of the Generation IV International Forum (GIF). The GIF promotes a new generation of sustainable, safe and cost-effective nuclear reactors which minimize the production of long-lived radioactive waste and reduce the risk of proliferation. HLMCRs are characterized by a fast neutron spectrum and have the potential to meet all the above-mentioned goals.

The design of the core of Lead-cooled Fast Reactors (LFRs) is a multidisciplinary task which deals with a large number of highly interconnected physical/engineering parameters. It can be logically subdivided into Thermal-Hydraulic (TH), Neutronic (NE) and Thermo-Mechanic (TM) design, based on the three most relevant physics involved. The approach to LFR core design currently adopted at ENEA embeds safety considerations from the early stages. The design procedure can be summarized as follows: technological constraints are first identified to derive design guidelines; individual components are then designed; interfaces with other reactor systems are then managed; eventually, the performances are optimized by working on the available margins with respect to the above-mentioned constraints [1]. The resulting design is then verified, possibly leading to further design iterations. This process is supported by Design-Oriented Codes (DOCs), i.e. fast-running codes with a clear application domain which can quickly and effectively inform design decisions by highlighting the relations between the parameters entering the specific problem.

Among the goals of the TH design of an LFR core exploiting the closed sub-assembly (SA) option, cold by-passes must be avoided and excessive thermal gradients among opposite faces of the assembly ducts prevented [2]. This requires a suitable coolant flow outside the assemblies themselves, i.e. along the Inter-Wrapper (IW)

gap, for which the width is established by the core TM design. Moreover, for wrapped assemblies, the possibility of tuning the IW flow fraction at the SA level by introducing flow restrictions arises, giving an extra degree of freedom to the designer for levelling thermal gradients at the assemblies' outlet. Therefore, the design process requires knowledge of the axial and radial coolant temperature profiles in the IW gaps throughout the whole core (i.e., including all core SAs), as well as of the axial and perimetrical wrapper temperature profiles, and notably the (possibly) different values of each side of the wrapper itself which could induce SA bowing.

A survey of the available literature pointed out the existence of at least four TH codes suitable for the full-core analysis of HLMCRs: COBRA-WC [3], NETFLOW [4], SUPERENERGY-2 [5] and its most recent version SE2-ANL [6]. However, COBRA-WC and NETFLOW are rather complex tools aimed at transient analyses, hence more suitable for the verification phase than for the design phase. SUPERENERGY-2 and SE2-ANL are closer to a DOC, thanks to their steady state nature, but the IW flow is treated in a somewhat simplified way. Therefore, to the best of the authors' knowledge, no DOC is currently available which satisfies the above-mentioned requirements, although it should be mentioned that DOCs for the TH simulation of the single SA such as ANTEO+ are able to account for the neighbouring IW coolant [7,8]. These considerations motivated the design and development of TIFONE, a DOC targeted at addressing the above-mentioned needs. The code has been preliminarily validated against experimental data collected at the KArlsruhe Liquid metal LAboratory (KALLA) within the framework of the SESAME H2020 project.

The paper is organized as follows: the approach followed for the code development, the simplified governing equations and the solution method shall be presented in section 2. The code validation shall be presented in section 3. Finally, conclusions and perspective for future applications and developments shall be presented in section 4.

2. THE TIFONE CODE

2.1. Code design overview

TIFONE targets the TH simulation of the IW coolant in LFRs exploiting the closed SA option in hexagonal geometry. The code name is based on an Italian acronym (Termo-Idraulica delle Fughe che Occorrono nel Nocciolo fra gli Elementi, which means "thermal-hydraulics of the bypass flow occurring in the core among the SAs"). The calculation domain, sketched in Fig. 1 (left), extends radially over the IW region of the entire core, and axially between the dividing and merging points of the inter- and intra-SA coolant flows. The sub-channel (SC) approach was chosen, since it allows to achieve a sufficient level of spatial resolution while retaining the key features of a DOC. The current version of TIFONE solves the inter-assembly coolant mass, energy and momentum equations, as well as the convection equations between the coolant and the wrapper. Among the perspective applications of TIFONE is the coupling with codes for the thermal-hydraulic analysis of the single SA, so to allow for a full-core TH simulation.

The code was developed according to the Software Quality Management System in place within ENEA's SICNUC division, which incorporates guidelines from standards such as ISO/IEC/IEEE 12207 [9]. After the initial planning phase, a software requirements specification document was produced. A software design compliant with the specified requirements was then developed, discussed and approved before starting the code development phase. This phase also embeds testing and verification activities, aimed at assessing the compliance of the code with the physical and functional requirements. Finally, the code was validated against available experimental data.

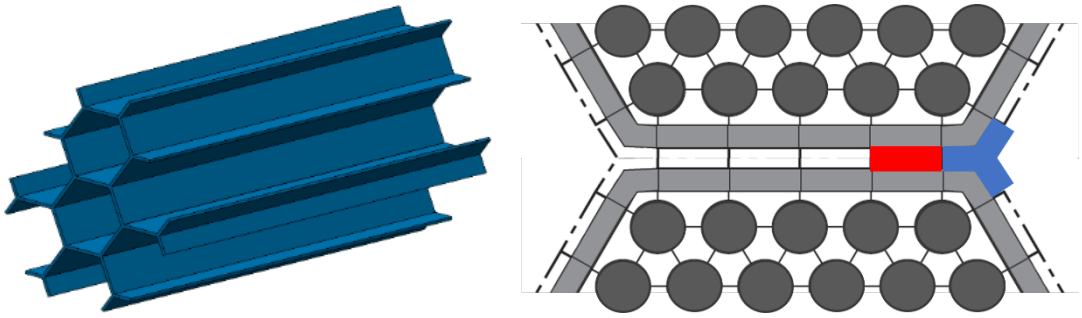

FIG. 1. Schematic representation of the IW flow domain (left) and SC discretization in the IW region (right).

2.2. Spatial discretization

The gap between adjacent SAs is radially subdivided into a number of SCs (called *edge SCs*), indicated in red in Figure 1(b). A second type of SCs, named *corner SCs* and indicated in blue in Fig. 1 (right), is associated with each of the junctions between three neighbouring gaps. This choice allows the TH connection between adjacent gaps to be taken into account, as well as to take advantage of the most detailed information available for the heat crossing the gap. This subdivision was adopted in the past in SUPERENERGY-2 [5]. The possibility to further split the IW gap between the neighbouring SAs, with boundaries at the centreline, has also been considered. However, this would provide an unnecessary level of detail, while potentially hindering code stability. This option has therefore been disregarded.

Each SC is axially subdivided into a number of control volumes which can be arbitrarily distributed according to the user input.

2.3. Governing equations

TIFONE aims at determining the TH behaviour of the inter-assembly coolant over the full core of an LFR, as well as the wrapper outer temperature for each SA. This is accomplished by adopting the SC method, using the discretization identified in the previous section. The underlying assumptions of the SC method, as indicated in [10] are:

- Fixed control volume, common to all conservation equations, except the transverse momentum conservation;
- For transverse flow (i.e., the flow between neighbouring SCs) does not have a vector direction, i.e. it "loses memory" of its original direction.

Additional simplifying assumptions have been adopted in the present work, aiming at a balance between code complexity and accuracy of the results, which is an essential feature of a DOC:

- The problem is solved in steady state, with no variable being integrated over time - meaning that a true steady state formulation is adopted, rather than different approaches such as a pseudo-transient;
- The IW channel cross section is axially constant. In an LFR core, the entrance and exit regions located at the bottom and top of the core, respectively, are actually characterized by an axially variable cross section. However, these regions - which are part of the computational domain - are not directly modelled. Therefore, the pressure drop due to the transition from bottom plenum to IW and from IW channel to top plenum (assuming upward flow) is accounted for by a localized pressure loss coefficient which can be determined, e.g., via 3D CFD calculations;
- Energy deposition by viscous dissipation in the coolant is neglected;
- Axial heat and momentum transfer via conduction and turbulent momentum flux, respectively, are neglected;
- The channel is assumed to be vertical, therefore gravity only contributes as a body force to the axial momentum balance;

In the following, the governing equations for the SC method are presented and simplified according to the above-mentioned assumptions for the problem at hand. The adopted boundary conditions are also indicated. The formulation is consistent with [12].

2.3.1. Mass conservation

Conservation of mass describes the axial variation of the mass flow rate in each SC. The mass flow rate for a given SC can change due to the net mass exchange with the neighboring ones. In general, this transfer can be caused by either pressure differences or density differences (buoyancy effects). In view of the above-mentioned assumptions, the mass conservation equation can be written as:

$$\frac{\Delta \dot{m}_i}{\Delta z} = -\sum_{j=1}^{N_{nei}} W_{ij} \tag{1}$$

where Δz is the SC axial length, $\dot{m} = \{\rho v A\}$ is the axial mass flow rate (where A is the cross-sectional SC flow area, ρ is the fluid density, v is the fluid velocity and the $\{\ \ \}$ operator represents a surface average over the flow area), and W is a mass flow rate per unit length in kg/m/s. Here and thereafter, the axial variation of a quantity ψ between z (i.e. the axial coordinate of the inlet of the control volume) and $z + \Delta z$ (i.e. the axial coordinate of the outlet of the control volume) is expressed as $\Delta\psi = \psi_{z+\Delta z} - \psi_z$. The subscript j denotes quantities related to one of the $N_{nei,i}$ neighbours of the i-th SC, N_{nei} being equal to 2 for *edge SCs* and to 3 for *corner SCs*. The subscript ij indicates exchange quantities between SC i and SC j.

The code takes in input both the total core mass flow rate and its repartition between the SAs and the IW region. Once the IW mass flow rate is known, TIFONE further subdivides it radially among the SCs. The approach for doing so depends on the choice concerning the treatment of the transverse momentum conservation equation, as described in section 2.3.4. The user is nevertheless left with the possibility to impose an arbitrary flow repartition among SCs in the IW region. This capability will, for example, allow the designer to test the effectiveness of an ad-hoc, local variation of the by-pass flow gagging scheme to tune the mass flow rate in a subset of the IW SCs.

2.3.2. Energy conservation

Conservation of energy describes the axial evolution of the coolant enthalpy in each SC. The enthalpy variation along a given SC is due to power absorbed in the SC, heat transfer with the portion of the wrapper wetted by the SC and net energy exchange with neighboring SCs. The latter can be caused either by net mass exchange (with the consequent energy transport) or by mixing effects which do not imply a net mass exchange, namely conduction and turbulent mixing. The energy conservation equation can be stated as follows:

$$\frac{\Delta(\dot{m}_i h_i)}{\Delta z} = A_i \dot{q}_{eq,i} - \sum_{j=1}^{N_{nei}} W_{ij}^{*H}\left(h_i - h_j\right) - \sum_{j=1}^{N_{nei}} W_{ij}\{h^*\} \tag{2}$$

where h is the fluid enthalpy, $\dot{q}_{eq}$ is the equivalent power per unit volume deposited in the SC due to either heat transfer with the adjacent SAs or the volumetric heat generation, W^{*H} is the effective mass flow rate per unit length for energy exchange and $\{h^*\}$ is an effective enthalpy transported by the cross flow (averaged over the contact area between SCs i and j).

In the IW region, the effective energy exchange between SCs i and j, $W_{ij}^{*H}\left(h_i - h_j\right)$, is in general associated to conduction and turbulence:

$$W_{ij}^{*H}\left(h_i - h_j\right) = q''_{ij} s_{ij}\big|_{cond} + q''_{ij} s_{ij}\big|_{turb} \tag{3}$$

where q'' is a heat flux and s is the width of the gap between adjacent SCs. The conduction contribution can be expressed as:

$$q''_{ij} s_{ij}\big|_{cond} = \bar{\rho}_{ij} s_{ij} \kappa_{ij} \left(\frac{\bar{\alpha}_{ij}}{\eta_{ij}}\right)\left(h_i - h_j\right) \tag{4}$$

where α is the fluid thermal diffusivity, η is the centroid-to-centroid distance between the SCs, $\kappa = \eta / l$ is the *conduction shape factor*, i.e. the ratio between the centroid-to-centroid distance and the *effective mixing length* l. Quantities characterized by a bar ($\bar{}$) are averaged between SCs i and j. Note that, to simplify notation, here and thereafter the volume average nature of the physical quantities appearing in the equations is not explicitly stated (e.g. $\bar{\rho}_{ij} = \left(\langle \rho_i \rangle + \langle \rho_j \rangle\right)/2$ would simply be written as $\left(\rho_i + \rho_j\right)/2$. The turbulent contribution can be characterized as follows:

$$q''_{ij} s_{ij}\big|_{turb} = W_{ij}^{T,H}\left(h_i - h_j\right) \tag{5}$$

where $W_{ij}^{T,H}$ is the effective mass exchange rate between adjacent SCs due to turbulent interchange. Chen [12] proposed to correlate $W_{ij}^{T,H}$ to the eddy diffusivity ε, thus writing:

$$W_{ij}^{T,H} = \bar{\rho}_{ij} s_{ij} \left(\frac{\varepsilon_{ij}}{\eta_{ij}} \right) \tag{6}$$

A literature review pointed out the lack of empirical correlations providing ε and κ for a geometry relevant for TIFONE. For this reason, $\varepsilon = 0$ (i.e. purely conductive internodal energy exchange) and $\kappa = 1$ are assumed.

The energy source term $\dot{q}_{eq,i}$ can be characterized as follows:

$$\dot{q}_{eq,i} = \dot{q}_i + \sum_{m=1}^{N_{w,i}} \frac{q''_{w,o,m} p_{h,m}}{A_i} \tag{7}$$

where the first term on the right-hand side, $\dot{q}_i$, is the heat deposited in the coolant per unit volume (e.g., due to gamma rays) and the second one represents the contribution of heat transfer with the wrapper. The summation runs over the number of wrapper walls in contact with the SC ($N_w = 2$ for *edge SCs* and $N_w = 3$ for *corner SCs*). $q''_{w,o,m}$ is the heat flux crossing the m-th wrapper outer surface (hence the subscript o) in contact with SC i. $p_{h,m}$ is the heated perimeter associated to the m-th wall in contact with SC i.

The inlet temperature distribution is specified by the user. Although it is straightforward to specify a uniform distribution, the user is free to assign a different value for each of the six gaps surrounding each SA. To ensure a suitable flexibility of the user input, the axial and radial discretization of the heat flux crossing the wrapper is allowed to be different from the one adopted for the control volumes. The heat source $q''_{w,o,m}$ for each control volume appearing in equation (7) is then determined via interpolation.

Although the space here available is insufficient to thoroughly describe the evaluation of thermophysical properties, it is worth mentioning that density, viscosity, specific heat, thermal conductivity and enthalpy are evaluated according to [11]. Although the code is targeted to HLMCRs, it is desirable to take advantage of past sodium experiments for validation purposes. For this reason, sodium properties were also included.

2.3.3. Axial momentum conservation

Conservation of axial momentum describes the axial evolution of momentum in each SC. According to the above-stated simplifications, axial momentum for a given SC can occur due to gravity, friction with the portion of the wrapper wetted by the SC, localized pressure losses and momentum exchange with neighbouring SCs. The latter can be caused by either net mass exchange (with the consequent momentum transport) or by mixing effects (which do not imply a net mass exchange). The axial momentum conservation can be stated as follows:

$$\begin{aligned} \frac{\Delta(\dot{m}_i v_i)}{\Delta z} = & -A_i \langle \rho_i \rangle g - A_i \frac{\Delta\{P_i\}}{\Delta z} - \sum_{j=1}^{N_{nei}} W_{ij}^{*M} (v_i - v_j) \\ & - \sum_{j=1}^{N_{nei}} W_{ij} \{v^*\} - \frac{1}{2} \langle \rho_i \rangle v_i^2 A_i \frac{f}{D_{H,i}} - A_i \frac{\Delta P_{form,i}}{\Delta z} \end{aligned} \tag{8}$$

where W^{*M} is the effective mass flow rate per unit length for momentum exchange, $\{v^*\}$ is an effective velocity transported by the cross flow (averaged over the contact area between SCs i and j), g is the gravitational acceleration, f is the friction factor with the walls, $D_H = 4A/p_w$ is the hydraulic diameter (where p_w is the wetted perimeter) and ΔP_{form} is the form (localized) pressure loss per unit length.

The effective momentum exchange term W_{ij}^{*M}, similarly to the W_{ij}^{*H} term encountered in equation (2), is composed by a molecular (diffusive) contribution and a turbulent contribution which is proportional to an equivalent mass flow rate for unit length. The molecular contribution to the axial momentum exchange between SCs is usually neglected [12]. The equivalent mass flow rate per unit length for turbulent contribution $W_{ij}^{T,M}$ is instead considered equal to its energy counterpart $W_{ij}^{T,H}$ and thus related to the eddy diffusivity concept. For simplicity, in the following it will be referred to simply as W_{ij}^{T}.

Several correlations for the friction factor f are implemented in TIFONE: those obtained by Blasius, Colebrook and Haaland for turbulent flow, as reported in [11], and a recent correlation by Liang [13] for laminar flow. To any of the above correlations that is selected to represent a reference circular duct, a corrective factor is introduced to account for the actual, non-circular shape of the considered SCs, following the guidelines from the Idelchik handbook [14].

The inlet pressure is specified by the user and assumed to be equal among all the SCs.

2.3.4. Transverse momentum conservation

Solving the transverse momentum conservation equation allows to account for the pressure-driven cross flow between neighboring SCs, which are typically significant in the case of flow blockages or axial variations of the flow area. This occurs at the expense of an increased code complexity. Since these physical situations are outside the application domain targeted by TIFONE, the radial pressure difference between SCs at a given axial coordinate has been neglected. The resulting transverse momentum conservation equation reduces to imposing an equal pressure drop among all the SCs for each axial step:

$$P_i = P_j \; \forall \; i, j \tag{9}$$

As the radial momentum equation has been reduced to the equality of the pressures among SCs for each axial level, no boundary conditions have to be imposed.

2.3.5. Flow split calculation

Due to the simplified treatment of the radial momentum conservation equation, a *flow split* model is required to determine the distribution of the IW mass flow rate among the various SCs. According to equation (9), all SCs share the same pressure drop. By enforcing this condition, a set of nonlinear equations is obtained having as unknowns the flow fractions for each SC i, $X_i = v_i/v_{ave}$, v_{ave} being the average velocity [1]. For incompressible flow in parallel hydraulic channels of constant cross section, this is tantamount to equating the sum of localized and distributed head losses for each SC:

$$v_i^2 \frac{f_i}{D_{H,i}} L + \xi_i v_i^2 = v_j^2 \frac{f_j}{D_{H,j}} L + \xi_j v_j^2 \tag{10}$$

where L is the total axial length of the domain and ξ is the sum of the localized pressure loss coefficients along a given SC. Since f, D_H and ξ are shared by SCs having the same shape – *corner* or *side* – and the same cross section, N_{cat} categories of SC are identified so to eliminate redundant equations. The resulting nonlinear system of equations is solved iteratively.

2.3.6. Heat transfer in the wrapper

Among the requirements for TIFONE, the axial distribution of the outer wrapper temperature must be determined, with a required radial resolution at least sufficient to distinguish each of the six sides of the wrapper. To this aim, the wrapper was discretized consistently with the SCs, see Fig. 1 (right). The outer wrapper temperature is computed as:

$$T_{w,o,m} = T_{sc} + q''_{w,o,m}/\alpha_o \tag{11}$$

Where T_{sc} is the mass flow averaged temperature of the IW coolant wetting wrapper surface m and α_o is the corresponding heat transfer coefficient. Following [11], correlations for the Nusselt number derived by Kays, Duchatelle, Dwyer and Sleicher/Rouse are implemented in TIFONE.

2.4. Flow regimes and solution method

The TIFONE application domain encompasses both the forced and the mixed convection regimes. According to Jackson [15], the criterion for determining the onset of significant mixed convection effect is the following:

$$Y_{mix} = Gr/Re^2 > 0.002 \quad (12)$$

Based on this figure of merit, TIFONE solves the equations listed above either according to the forced convection approximation, completely neglecting buoyancy-driven inter-SC mass transfer, or considering mixed convection effects. In the latter case, the solution method proposed by Chen has been adapted to the specific problem at hand [12]. It should be mentioned that, as already pointed out by the developers of SUPERENERGY-2 [5], the forced convection solution in the IW domain is severely limited by stability issues. For this reason, the consistency of the mixed convection solution with the forced convection solution for $Gr/Re^2 \ll 0.002$ has been verified, so that the mixed convection solution approach can be used in place of the forced convective one in case stability issues occur. The consequent increase in computational time does not prevent the code from running fast enough to be useful during the core design phase (less than a minute of single-core runtime for a full core calculation performed on a laptop).

3. PRELIMINARY VALIDATION

Code validation against experimental data is essential to quantify the confidence in the code predictions within the anticipated validity domain. In this section, the application of TIFONE to the simulation of recently performed experiments at the KALLA facility is presented, together with the comparison with available measurements.

3.5. Experimental setup

Experiments performed at the KALLA facility in the framework of the SESAME project aimed at providing detailed thermal measurements for the IW flow and heat transfer in the gap between three SAs cooled by Lead-Bismuth Eutectic (LBE). The experimental record is reported in a SESAME deliverable [16] and selected results are contained in a related paper [17]. Fig. 2 (left) shows a cross-section of the test section.

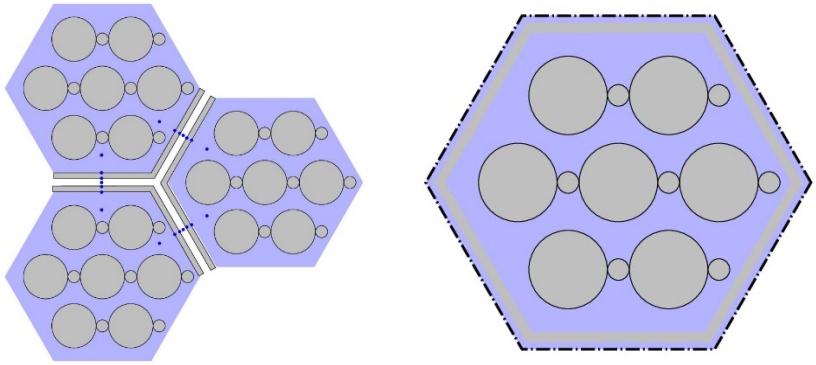

FIG. 2. Thermo-couple location for each measurement level in KALLA facility, reproduced from [16] (left) and simulation setup for the ANTEO+ calculation (right).

The main geometrical parameters of the test section, which were chosen according to a scaling of the MYRRHA-7 design values, are reported in Table 1.

Available measurements include: the radial temperature distribution at two selected axial locations with the sensor layout indicated in Fig. 2 (left); the axial temperature distribution along the only corner present in the setup; the axial temperature distribution at a radial location corresponding to the barycentre of each wing; the local velocity and temperature profiles at the outlet section of gap AB; the radial temperature distribution at the outlet of the test section along the gaps AB and BC.

TABLE 1. MAIN GEOMETRICAL PARAMETERS OF THE KALLA IW FLOW TEST TECTION [16].

Category	Quantity	Unit	Value	Meaning
Outer dimensions	FF	mm	65.00	Outer flat-to-flat distance
	w	mm	2.0	Wall thickness
	δ	mm	3.0	Gap width
Bundle dimensions	D	mm	16.0	Rod diameter
	L_{heat}	mm	600.0	Rod heated length
	L_{tot}	mm	1400.0	Rod total length
	P	mm	20.50	Rod pitch
	d	mm	4.40	Wire diameter
	H	mm	262.0	Wire pitch
	W	mm	20.75	Pin-Wall distance
Flow areas	A_{bdl}	mm^2	1704.2	Bundle channels (A-C)
	A_{gap}	mm^2	331.9	Gap channel (D)
Hydraulic diameters	$d_{h,bdl}$	mm	10.31	Bundle channels (A-C)
	$d_{h,gap}$	mm	5.85	Gap channel (D)

3.6. Results and discussion

3.6.7. Symmetric case 1

Case 1 is symmetric, i.e., the heating and cooling parameters of the three SAs are the same. The input data for TIFONE are summarized in Table 2.

As a first approximation, the axial distribution of the heat flux crossing each wrapper face $q''(z)$ was computed via a standalone ANTEO+ simulation. ANTEO+ was not designed to handle physical situations where only two out of six wrapper faces are cooled by the IW, therefore a symmetric cooling had to be assumed, see Fig. 2 (right). Although it was verified that the computed total power discharged to the IW coolant was consistent with the one measured via calorimetry, the adopted simulation setup does not allow to consider effects such as the distortion of the internal SC temperature distribution associated to the presence of the adiabatic wrapper faces. Moreover, local effects such as spatially periodic temperature variations associated to the presence of the wire could not be accounted for. It should be remarked that resorting to an external tool was necessary to compensate for the unavailability of detailed measurements of the heat flux distribution over the surfaces facing the IW gap, which is a necessary input for TIFONE. This is however relevant for the perspective application of TIFONE, i.e., the self-consistent coupling to SA codes such as e.g., ANTEO+ to achieve a full-core TH solution.

The mixed solution method was employed, even though the value of Gr/Re^2 was slightly lower than the suggested value for the onset of buoyancy effects.

TABLE 2. TIFONE INPUT DATA FOR VALIDATION CASES

Quantity	Unit	Case 1	Case 4	Case 6	Case 8	Case 93
$\dot{m}$ – IW mass flow rate	kg/s	0.686	0.517	0.342	0.17	0.516
T_{in} – Inlet LBE temperature	˚C	199.25	199.20	199.10	199.10	199.98
q_{tot} – Total power to IW flux	kW	3.700	3.010	2.160	1.170	2.720
q'' – Surface heat flux	kW/m^2	$q''(z)$	$q''(z)$	$q''(z)$	$q''(z)$	See Table 3

Fig. 3 (left) shows the computed and measured axial temperature profile along the gap SC, whereas Fig. 3 (right) shows the computed and measured axial temperature at locations placed at the half length of each side. Comparison with experimental data points suggests that the axial shape of the heat flux crossing the wrapper is incorrectly approximated. This is a consequence of the above-mentioned approximations in the ANTEO+ simulation setup, which shall be removed in future work.

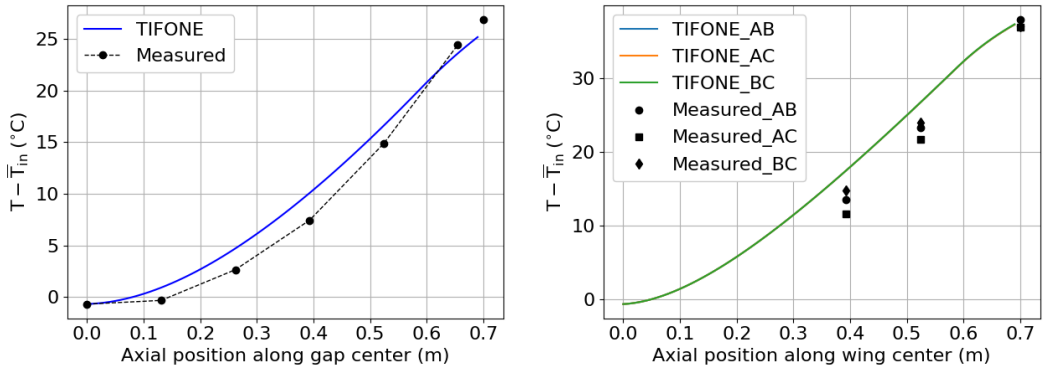

FIG. 3. Computed and measured axial evolution of the temperature increase at the centre of the IW region (left) and at the centre of each gap (right) for Case 1.

Fig. 4(a) and Fig. 4(b) show the comparison between the computed and measured temperatures and velocity, respectively, at the outlet section. It should be noticed that, due to the symmetric boundary conditions provided to TIFONE, the fact that the curves corresponding to the three wings are superimposed can be considered as a sanity check. The experimental values, instead, show some differences which are likely due to local effects associated e.g. to the presence of the wire. The comparison between the computed and measured temperatures shows a very good agreement. As for the velocities, only measurements along wing AB were available. The measured values appear to be always larger than the computed ones. This can be caused by the local nature of the velocity measurements, catching the value at the gap centerline, whereas TIFONE computes an average SC velocity. Moreover, the cusp computed at 5 mm from the gap center is a nonphysical behavior following from having neglected the inter-SC friction. This will be the subject of future investigations, possibly relying on experiments or detailed calculations to derive correlations for the eddy diffusivity in the considered gap geometry.

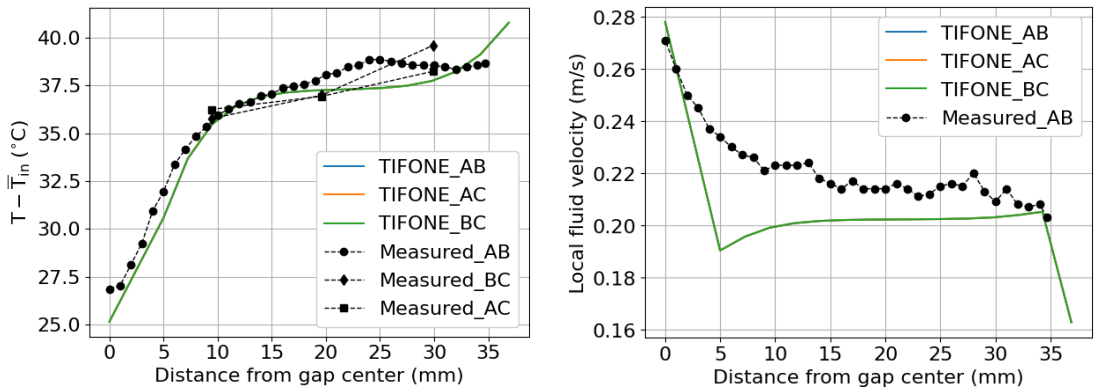

FIG. 4. Computed and measured temperature profiles at gap outlet for case 1.

3.6.8. Other symmetric cases

The three further symmetric cases here considered, numbered as 4, 6 and 8 in [16], are characterized by a progressive reduction in both the IW coolant flow rate, in turn resulting in reduced heat losses from the SAs. As for case 1, the mismatch in the axial temperature evolution shown in Fig. 5 is believed to follow from the approximate calculation of the axial heat flux distribution. Nevertheless, Fig. 6 shows a very good agreement on the temperature profile along the AB gap for cases 4 and 6. For case 8, instead, the agreement is bad. Indeed, due to the low flow rate, buoyancy effects play a dominant role, meaning that the mixed convection assumption is no longer valid, thus falling outside the TIFONE application domain.

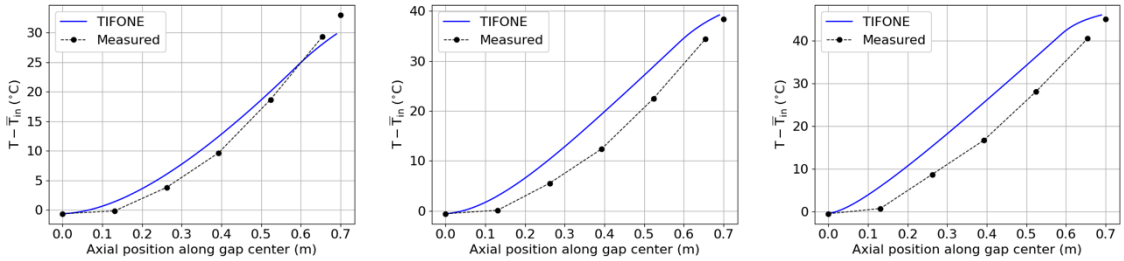

FIG. 5. Computed and measured axial evolution of the temperature increase at the centre of the IW region for cases 4 (left), 6 (centre) and 8 (right).

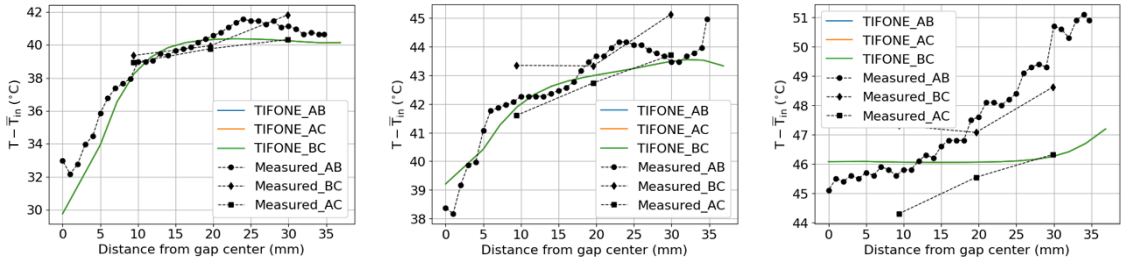

FIG. 6. Computed and measured temperature profiles at gap outlet for cases 4 (left), 6 (centre) and 8 (right).

3.6.9. An asymmetric case

Due to space constraints, only one asymmetric case is here reported, namely case #93. Here, the asymmetry is induced by heating the three SAs in the test section uniformly, while completely hindering the mass flow rate within SA C, leading to non-negligible inter-SA heat transfer. In this case, the flow and heat transfer inside SA C are dominated by natural circulation. These effects cannot be accounted for in the ANTEO+ model for the single SA which was proposed for the symmetric case. For this reason, available calorimetric measurements have been employed to retrieve the fraction of the total power transferred to the IW coolant which is associated to each SA. This value was then divided by the area of each wrapper face facing the IW coolant, yielding the heat flux values reported in Table 3. These values have been assumed as axially uniform, as a very first approximation.

TABLE 3. HEAT FLUX VALUES FOR EACH WRAPPER FACE FOR THE ASYMMETRIC CASE

q''_{AB}	q''_{BC}	q''_{AC}	q''_{BA}	q''_{CB}	q''_{CA}
10.11	22.80	21.01	10.11	22.80	21.01

The good agreement between the computed and measured axial evolution of the temperature difference along the *corner SC* shown in Fig. 5 (left) could be associated to the fact that the heat flux from SA C, which is the most significant one, is more uniform with respect to the case of forced convection flow. The radial temperature profile at the outlet is in satisfactory agreement with experimental data, see Fig. 5 (right).

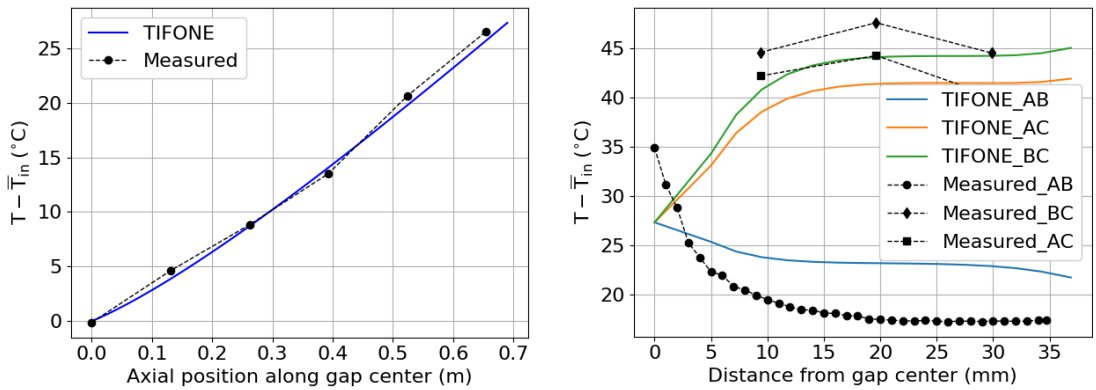

FIG. 7. Computed and measured axial evolution of the temperature increase at the centre of the IW region for the asymmetric case (left) and temperature profiles at the gap outlet (right).

4. CONCLUSIONS AND PERSPECTIVE

The design, development and preliminary validation of a new DOC, the TIFONE code, was successfully carried out. The models, methods and validation for the TIFONE code were described, together with a hint to the robust approach to quality-compliant development of a DOC aimed at supporting the core design of HLMCRs.

While the presented results are encouraging, further work is necessary to extend the applicability of TIFONE and to validate its capabilities of reproducing experimental data within the specified validity range. As for constitutive relations, the results here reported point out the need for eddy viscosity correlations which are relevant for the IW geometry. Such correlations could be derived via dedicated experimental campaigns or via suitable experiments. As far as the code extension is concerned, a version 1.1 of TIFONE is foreseen, which will be capable of launching many instances of a SA code such as ANTEO+ (one for each SA in the core), thus obtaining a full-core TH solution which can effectively support core design. Finally, as far as the code qualification is concerned, two lines of activity are foreseen:

(a) A benchmark against CFD simulations performed adopting the porous medium approach and considering the ATHENA facility [19] is foreseen, to test TIFONE in a reactor-relevant geometry;
(b) Other facilities including IW flow and heat transfer effects are planned, including CLEAR-S [18] and ATHENA itself. The resulting datasets shall be employed for further validating TIFONE, with specific focus on effects associated with multi-SA configurations.

REFERENCES

[1] LODI, F., Development of Core Design Methods and Tools for Gen-IV Heavy Liquid Metal Cooled Reactors, Ph.D. thesis, UniBO (2017).

[2] INTERNATIONAL ATOMIC ENERGY AGENCY, Structural Materials for Liquid Metal Cooled Fast Reactor Fuel Assemblies – Operational Behaviour, Nuclear Energy Series No. NF-T-4.3, IAEA, Vienna (2012).

[3] GEORGE, T.L., COBRA-WC: A Version of COBRA for Single-Phase Multiassembly Thermal Hydraulic Transient Analysis, internal report, Pacific Northwest Laboratory, Richland, Washington 99352, 1980.

[4] MOCHIZUKI, H., Inter-subassembly heat transfer of sodium cooled fast reactors: Validation of the NETFLOW code, Nucl. Eng. Des. **237** (2007) 2040-2050.

[5] BASEHORE, K. L., SUPERENERGY-2: A Multiassembly, Steady-State Computer Code for LMFBR Core Thermal-Hydraulic Analysis, internal report, Pacific Northwest Laboratory, Richland, Washington 99352, 1980.

[6] YANG, W.S., "Assessment of the SE2-ANL code using EBR-II temperature measurements", 7th International Meeting on Nuclear Reactor Thermal-Hydraulics (Proc. Int. Conf. Saratoga Springs, NY, 1995), American Nuclear Society (1995).

[7] LODI, F., GRASSO, G., MATTIOLI, D., SUMINI, M., ANTEO+: A subchannel code for thermal-hydraulic analysis of liquid metal cooled systems, Nucl. Eng. Des. **301** (2016) 128-152.

[8] LODI F., GRASSO, G., Extension of the sub-channel code ANTEO+ to the mixed convection regime, Nucl. Eng. Des. **322** (2017) 368-378.

[9] International Organization for Standardization. (2017). Systems and software engineering — Software life cycle (ISO/IEC/IEEE Standard No. 12207:2017). https://www.iso.org/standard/63712.html

[10] TODREAS, N.E., Nuclear Systems I – Thermal Hydraulic Fundamentals, CRC press (2021).

[11] NUCLEAR ENERGY AGENCY, Handbook on Lead-bismuth Eutectic Alloy and Lead Properties, Materials Compatibility, Thermal-hydraulics and Technologies – 2015 Edition, NEA No. 7268, NEA, 2015.

[12] CHEN, S., Constitutive correlations for wire-wrapper subchannel analysis under forced and mixed convection conditions, Ph.D. thesis, Massachusetts Institute of Technology, 1984.

[13] LIANG, Y. et al., Experimental and numerical investigation on flow characteristics of inter-wrapper channel in LMFBR, Ann. Nucl. Ene. **151** (2021) 107918.

[14] IDELCHIK, I.E., Handbook of hydraulic resistance - 3rd edition, CRC Press, Boca Raton, FL (1994).

[15] JACKSON, J.D., Turbulent mixed convection heat transfer to liquid sodium, Int. J. Heat Fluid Flow **4** 2 (1983) 107-111.

[16] PACIO, J. et al., KALLA Inter-wrapper flow experiments, internal report, Karlsruher Institut für Technologie (KIT), Karlsruhe, 2019.

[17] PACIO, J. et al., Experimental study of the influence of inter-wrapper flow on liquid-metal cooled fuel assemblies, Nucl. Eng. Des. **352** (2019) 110145.
[18] WU, Y., CLEAR-S: an integrated non-nuclear test facility for China lead-based research reactor, Int. J. Energy Res. **40** 14 (2016) 1951-1956.
[19] ROZZIA, D. et al., Technological installation of ATHENA and CHEM-LAB, internal report, Technical Report ENEA LR-D-S-190, 2015.